Journal of Visualization, Vol. 2, No. 2 (1999) 143-151

Visualization of Complex Near-body Transport Processes in Flexible-body Propulsion

Wolfgang, M. J.*, Triantafyllou, M. S.* and Yue, D. K. P.*

* Department of Ocean Engineering, Massachusetts Institute of Technology, Cambridge, Massachusetts 02139, USA.

Received 17 February 1999.
Revised 15 June 1999.

***Abstract*:** Recent interest in the application of fish-like propulsion mechanisms to practical engineering systems has led to the development of a three-dimensional numerical method to enable the study of the fluid dynamics associated with flexible-body swimming. Visualization of the near-body and near-wake flow processes has elucidated unique flow manipulation capabilities utilized by the fish, associated with the controlled production and release of body-generated vorticity. In addition, efficient actuation of flow into the oscillating tail allows for energy recovery by the tail from flow perturbations initiated by the upstream flexible-body motions for improved efficiency. In this work, we highlight some of these processes through visualization of the unsteady flow patterns, whose three-dimensionality is more complex than linear theory would suggest. We then compare these results to experimental data of fish swimming dynamics. These comparisons reinforce the applicability of the simulation method as a visualization tool for the study of the hydrodynamic mechanisms of fish-like swimming motions.

***Keywords*:** fish, vorticity control, flexible-body swimming, unsteady propulsion.

1. Introduction

In recent years, the interdisciplinary interest in the swimming of fish has yielded a wealth of research contributions from both fluid dynamicists and marine biologists alike. With the reported outstanding performance of fish straight-line swimming and unsteady maneuvering motions (Gray, 1936; Weihs, 1972, 1973; Aleyev, 1977; Videler and Hess, 1984; Harper and Blake, 1989; Domenici and Blake, 1997; Müller et al., 1997; Barrett et al., 1999; Wolfgang et al., 1999), understanding the mechanisms utilized by fish may be of great significance to unsteady marine propulsion technology (Triantafyllou et al., 1996). Several comprehensive works on fish swimming thoroughly analyze the kinematics and the dynamics of fish-swimming motions for a variety of species (Videler 1993; Blake 1983), but the flow mechanisms contributing to the performance are not fully understood.

Several theories have been developed to understand fish swimming performance (Wu, 1961, 1971; Lighthill, 1975). While these seminal works provide insight into the basic swimming propulsive mechanisms, the details of the three-dimensional flow and the dynamics of the shed vorticity are still not well known. Several other investigators have examined the propulsive characteristics of oscillating hydrofoil surfaces for both swimming and flying (Kármán and Burgess, 1935; Lighthill, 1975; Chopra, 1976; Chopra and Kambe, 1977; Lan, 1979; Ellington, 1984) and have identified the ability to generate large lift forces using such propulsive methods. However, these methods have not resolved some of the complex flow control mechanisms and do not describe the interaction effects of coupling this propulsion scheme to an upstream body.

Several investigators have studied the mechanisms of vorticity control achieved by unsteady motion of a body in a fluid. Taneda and Tomonari (1974) examined the flow around a flexible plate with a traveling wave of phase speed c_p in a free stream of velocity U and showed boundary layer turbulence suppression for $c_p > U$. An oscillating foil has been utilized to demonstrate energy recapture from eddies generated upstream in a shear flow,

with high propulsive efficiencies (Gopalkrishnan et al., 1994; Streitlien et al., 1996; Anderson et al., 1998). These mechanisms of boundary layer relaminarization and vorticity control by an oscillating tail fin contribute to the drag reduction and high propulsive efficiencies observed through direct dynamical measurements on a swimming fish-like robotic vehicle (Barrett et al., 1999). The manner in which these mechanisms of vorticity control are employed during fish swimming has proved elusive. Although recent improvements in experimental visualization techniques have allowed several investigators to examine the in-plane particle dynamics of the flow around actively-swimming live fish (Anderson, 1996; Müller et al., 1997), the correlation of the flow dynamics and the body kinematics to the instantaneous forces on the fish is only partially understood. Recent work by Wolfgang et al. (1999) presents a synergistic approach to recovering these dynamics through simultaneous experimentation and computation on a small fresh water fish, the Giant Danio (*Danio malabaricus*).

In this paper, we utilize a three-dimensional computational method to describe the unsteady flow about an actively-swimming, long-range, high-performance predator species, the bluefin tuna *thunnus thynnus*. We consider the steady, straight-line swimming motions of the bluefin tuna for prescribed kinematic parameters. The computed forces on the body are compared to the measured swimming dynamics of the bluefin tuna using the robotic underwater flexible hull vehicle, *RoboTuna*, constructed by Barrett (1996), since direct dynamical measurements of live tuna are difficult to obtain. Visualization of the wake structures and the near-body hydrodynamics resulting from the motions elucidate mechanisms by which the tuna manipulates the flow through the oscillation of the high-aspect-ratio caudal fin and releases body-generated vorticity into the wake, efficiently producing a reverse Kármán street thrust jet.

2. Method

A computational model is developed to simulate the flow kinematics and the forces around a three-dimensional, flexible, streamlined body with a rigid, sharp-trailing-edged, high-aspect-ratio caudal fin. We study through simulation the problem of this body starting from rest to a constant horizontal velocity U while undergoing periodic undulations about its mean line within an inviscid, incompressible fluid. An arbitrary number of thin shear layer wakes are allowed to separate from predefined separation lines, such as the trailing edge of the caudal fin, continuously as time progresses. The flow is assumed to be irrotational with the exception of the thin wakes, allowing for the existence of a velocity potential $\Phi(\vec{x},t)$. A three-dimensional time domain panel method based on Green's theorem is employed to solve for the velocity potential on the body and in the wake. Constant-strength, flat quadrilateral panels are chosen for the geometric representations, allowing for rapid computational time given the unsteady nature of the geometric influence coefficients (Katz and Plotkin, 1991). Using this method, the characteristics of the live tuna swimming at large Reynolds numbers are approximated by assuming that viscous effects are confined to a thin boundary layer and wake region. A desingularized formulation (Krasny, 1986) allows the shed wake surfaces to evolve and interact, affecting the performance of the motions. The implementation of this numeric scheme is an order of magnitude more rapid than the fully viscous numerical methods which are essential for examining fish-like motions at lower Reynolds numbers (Liu et al., 1997). The complete details of the formulation, implementation, and convergence of the computational scheme employed are developed in Wolfgang (1999).

The geometric and kinematic parameters used are identical to those used in the experiments with the robotic vehicle, *RoboTuna*, developed by Barrett (1996), and closely emulate those found in nature (Fierstine and Walters, 1968; Dewar and Graham, 1994). Several key kinematic parameters fully describe the motion of the body, which is characterized by a traveling backbone wave of smoothly-varying amplitude and phase speed c_p which differs from the swimming speed U. The leading edge of the articulated caudal fin follows the path of the necking rear portion of the body, the caudal peduncle. Additionally, the fin is allowed to assume an angle of attack α with respect to the path of the caudal penduncle, and temporal phase angle ϕ between the angular and lateral motions of the fin leading edge determines the point of maximum α during the tail lateral excursion cycle. The backbone waveform $y(x)$ can be written

$$y(x,\, t) = a(x) \sin(k\, x - \omega\, t) \tag{1}$$

$$a(x) = c_1\, x + c_2\, x^2 \tag{2}$$

where $k=2\pi/\lambda$ is the wavenumber, corresponding to wavelength λ, ω is the circular frequency of oscillation, and x is centered a distance 35% of the body length from the nose, with positive x in the direction from the nose to the tail. The amplitude envelope $a(x)$ is defined with adjustable parameters c_1 and c_2. We chose c_1 to be independent and dimensionless, while c_2 is chosen to achieve a specific value of the double-amplitude of motion, denoted by A, at the tail. The frequency scaling of data observed in fish is based on the wake Strouhal law (Triantafyllou et al., 1991, 1993), i.e. keeping constant the non-dimensional parameter *St:*

$$St = f A/U \tag{3}$$

where f is the frequency of oscillation and A is the average total lateral excursion of the tail fin.

The computational wake shedding parameters are chosen to examine the importance of upstream vorticity shedding on the wake and flow structure interactions with the body and on the subsequent performance of the tuna swimming motions. On the *RoboTuna*, the tail produces the largest wake, and the smooth elliptical cross sections of the body do not promote flow separation from any other sharp edges. However, real bluefin tuna have a ridge of finlets along the dorsal and ventral regions where the body cross section decreases, promoting upstream wake separation and interaction with the caudal fin. As a result, our computational model investigates (i) caudal fin shedding only, as might be found in the *RoboTuna*, and (ii) caudal fin and backbone ridge shedding, such as might be found on live tuna.

3. Results

We choose a simulation with kinematic parameters which resulted in excellent performance of the *RoboTuna* under conditions of self-propulsion. This motion experimentally resulted in a reduction of the drag on the actively-swimming body to 47.7% below the rigid body drag (Barrett et al., 1999). Kinematic parameters for this run: Strouhal number St=0.182, swimming speed U=0.656 BL/s, tail circular frequency ω=6.278 rad/s, wavelength λ=0.936 BL, tail tip double amplitude A=0.120 BL, angle of attack α=24.8 deg, tail phase between pitch and heave ϕ=80.0 deg, and amplitude parameters c_1=0.00294 and c_2=0.1375 BL^{-1}. The body length of the *RoboTuna* is BL=1.2 m, and the wetted surface area is S=0.5936 m^2.

Figure 1 shows the simulated motions over one-half of the swimming cycle. The two wake shedding schemes are shown for comparison, illustrating the self- and body-interaction effects of the deforming wakes. Visualization of computational fluid-structure interactions is achieved using Amtec TECPLOT. As can be seen from the color contours of wake dipole strength superimposed on the computational grid of the shed wake surfaces, the phase of encounter between the oscillating caudal fin and the body-generated vorticity released upstream through backbone ridge separation significantly affects subsequent wake-wake interaction dynamics. This phase of encounter is dependent on the wavelength of the backbone wave λ, the longitudinal distance between the backbone ridge and the leading edge of the caudal fin, and the phase speed of the backbone wave with respect to the swimming speed c_p/U. From Fig. 1, as the tail sweeps from side-to-side, a wake of oscillating strength separates from the caudal fin trailing edge. When the tail encounters the wake sheets shed upstream from the backbone ridge, the caudal fin wake induces a rotational velocity which is in the opposite direction of the fluid rotation induced by the upstream-shed vorticity. In this manner, the tail may recover energy released into fluid upstream and enhance the loading on the tail.

Figure 2 illustrates the interaction of fluid structures produced during the swimming motions for the two different shedding schemes. From the three-dimensional unsteady velocity field $\vec{v}(\vec{x},t)$, iso-surfaces of vertical vorticity ω_z and dynamic pressure coefficient Cp are extracted and shown over half of a swimming cycle, where $Cp=|\vec{v}(\vec{x},t)|^2/U^2$. The red and blue patches of vertical vorticity ω_z induce counter-rotating fluid velocity regions which define the boundaries of a reverse Kármán street thrust jet in the wake of the swimming fish. The regions of low pressure are formed upstream of the wake through the undulation of the body and the oscillation of the tail. These low pressure regions are then enhanced and manipulated by the tail, interacting with low pressure regions formed by the alternating-strength patches of wake vorticity ω_z. This further amplifies the fluid jet defined by the reverse Kármán street in the wake. The vertical vorticity ω_z are generally of constant diameter over the depth of the fish, reinforcing the predisposition of fish to swim at a Strouhal number St corresponding to the maximum spatial amplification of the two-dimensional thrust jet instability (Triantafyllou et al., 1993).

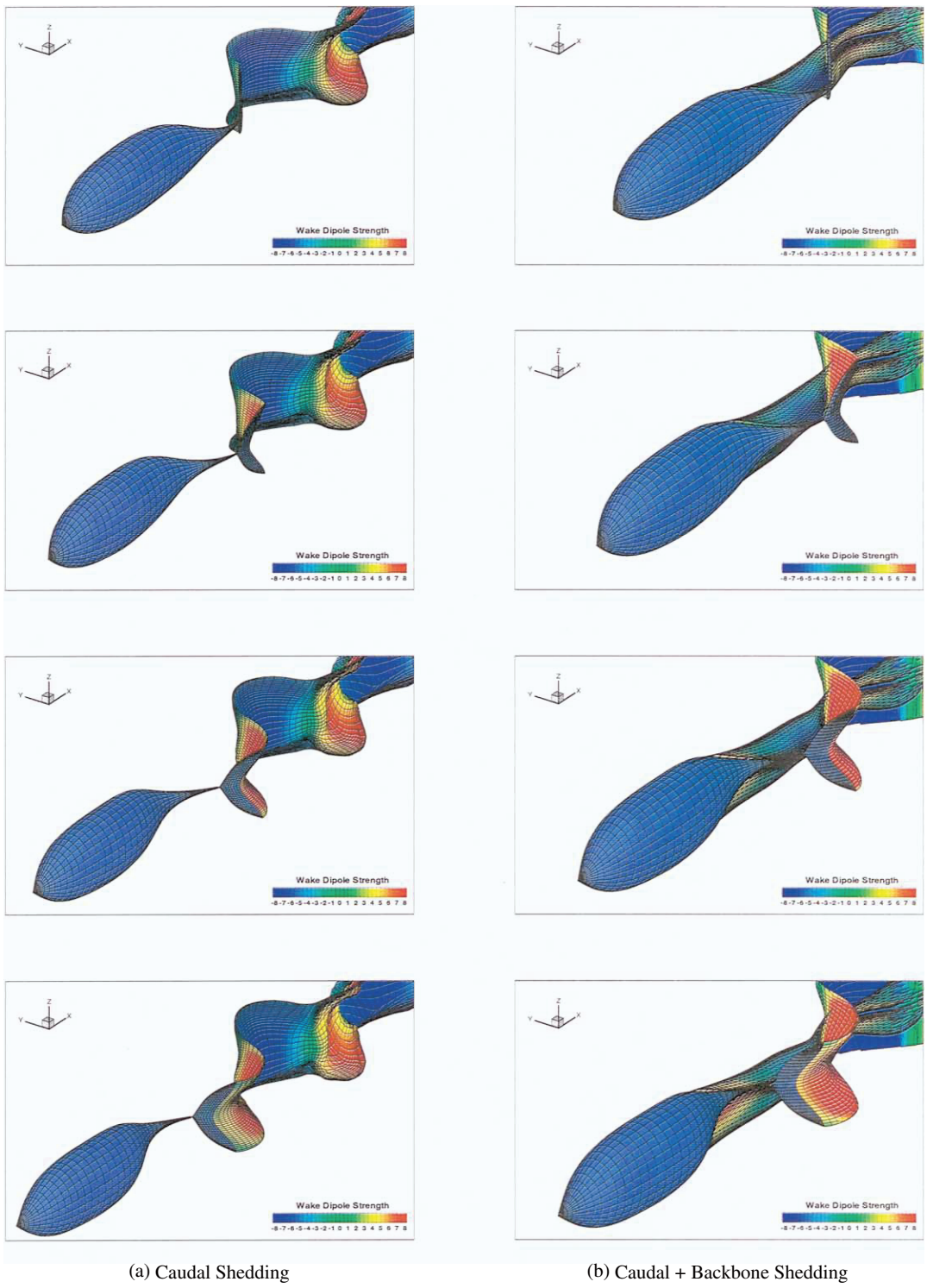

(a) Caudal Shedding (b) Caudal + Backbone Shedding

Fig. 1. Straight-line swimming motion simulation results for one-half of the swimming cycle showing wake interactions. Two different wake shedding schemes are shown for comparison: left column (a) employs caudal fin shedding only; right column (b) employs caudal fin and backbone ridge shedding. The computational grid is superimposed on the tuna geometry and the wake surfaces. Wake surface color is scaled by strength of the wake dipole sheet. Sequence for each column is shown top to bottom at intervals of $T/8$.

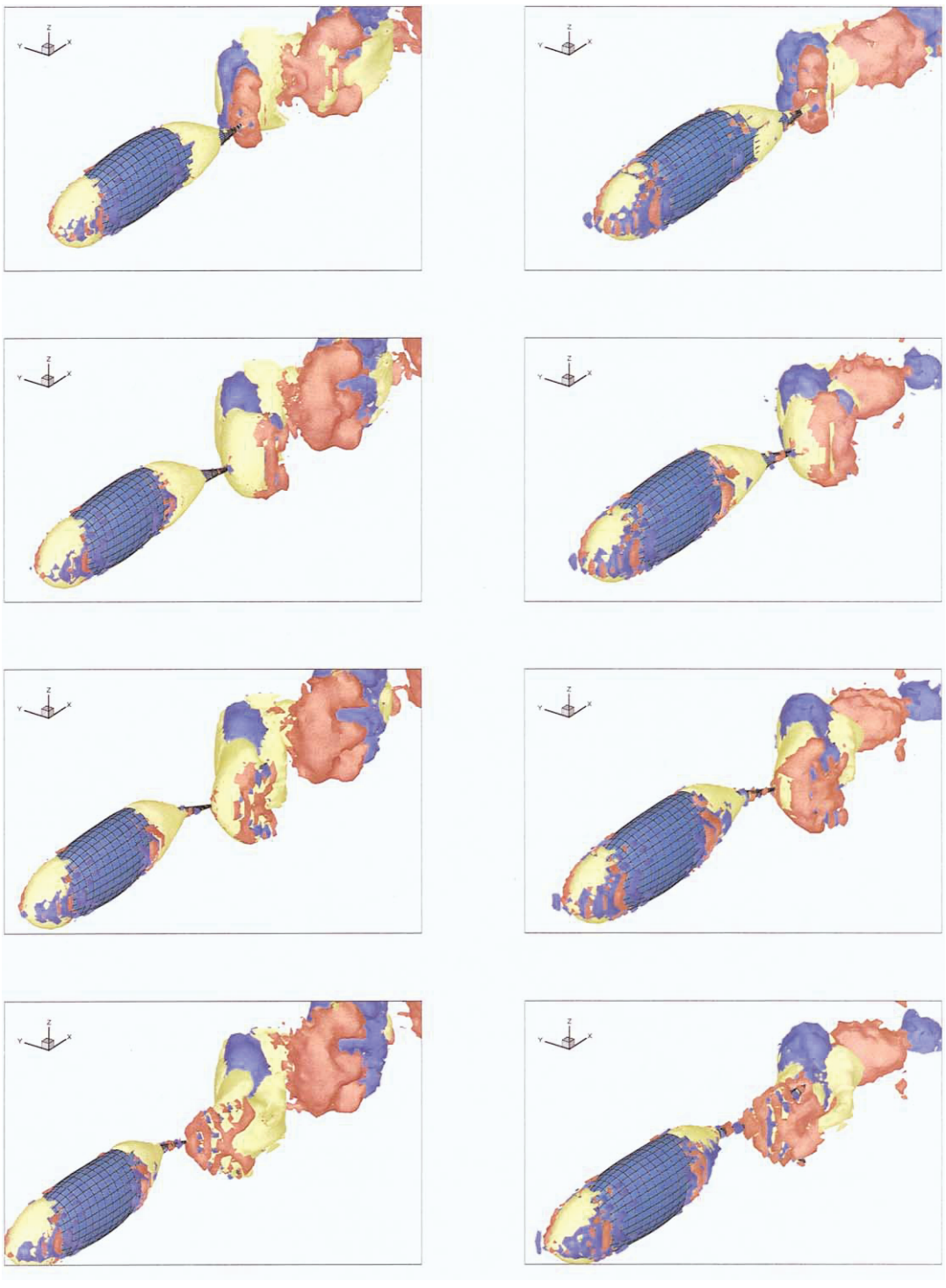

(a) Caudal Shedding (b) Caudal + Backbone Shedding

Fig. 2. Straight-line swimming motion simulation results for one-half of the swimming cycle showing flow structure interactions, employing (a) caudal fin shedding only and (b) caudal fin and backbone ridge shedding. Iso-surfaces of vertical vorticity ω_z are shown in red (ω_z = 1.0 s^{-1}) and blue (ω_z = −1.0 s^{-1}), and an iso-surface of dynamic pressure coefficient is shown in yellow(C_p = 0.8), nondimensionalized by the swimming speed U. The computational grid is superimposed on the tuna geometry. Sequence for each column is shown top to bottom at intervals of T/8.

Although the wake vorticity defining the thrust jet appears to have a two-dimensional structure, the near-body flow around the fish is much more complex. Linear theory would suggest that the streamlines of the velocity field would remain in-plane. Two-dimensional predictions for fish swimming dynamics require the flow velocities to remain in the longitudinal plane for all depths (Wu, 1961, 1971), whereas slender-body theory requires that the fluid velocity vectors remain in sectional planes along the body length (Wu, 1971; Lighthill, 1975). From Fig. 3, we can see that the actual flow along the fish length is quite complex. The flow profiles around the fish are shown at two depth planes, near the top of the body z/D=0.2 and along the mid-body depth z/D=0.5 for total body depth D, for the two wake shedding schemes. The in-plane velocity vector streamlines are superimposed on a contour plot of the vertical vorticity ω_z component in that plane. Again, we can see the two-dimensional nature of the wake vorticity structures from identification of the red and blue regions of alternating-strength vorticity at different depths, which induce the counter-rotating fluid velocity regions forming the reverse Kármán street thrust jet. Streamlines in the wake further identify the thrust jet of fluid, although wake-wake interactions resulting from implementation of the backbone ridge shedding model may make this less clear. However,while the flow around the body is characterized by the longitudinal patterns predicted by two-dimensional swimming theory, the confluence of the streamlines in some regions indicates a strong out-of-plane velocity component, suggesting a highly three-dimensional fluid actuation process affected by the fish motions.

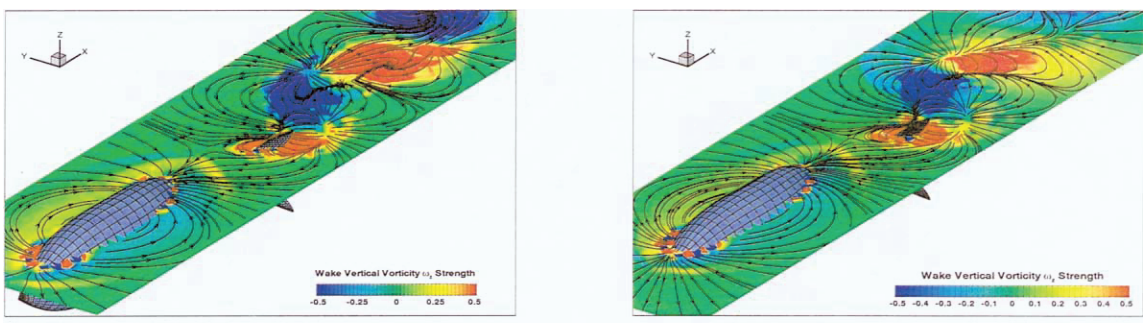

(a) Caudal Shedding (b) Caudal + Backbone Shedding

Fig. 3. Flow profiles at two vertical locations along the body of total depth D for (a) caudal fin shedding and (b) caudal fin and backbone ridge shedding. Top row: z/D=0.2 measured from the top. Bottom row: z/D=0.5. In-plane velocity vector streamlines (black) are superimposed on a contour plot of the vertical vorticity ω_z component in the plane (Range: [-0.5 s^{-1},0.5 s^{-1}]). Viewed from above, red vorticity indicates clockwise fluid rotation, blue vorticity indicates counterclockwise rotation, and green regions are irrotational. Time instant shown corresponds to the body position shown along the bottom rows of Figs. 1 and 2.

To further understand the impact of these fluid-body interactions revealed through our flow visualizations on the body dynamics, we compare our simulation results to the integrated performance dynamics obtained by the *RoboTuna*. In the absence of significant flow separation in the experiments, our computational method employing proper modeling of the self-induced wake dynamics is expected to provide reasonable estimates of the power needed by the fish-like body once the kinematics are specified. Fig. 4 (a) shows the power required for swimming by the experimental robotic vehicle under conditions of self-propulsion, compared to the power delivered to the fluid through simulation utilizing the two wake separation schemes. In addition, while thrust and drag cannot be measured separately in the experimental mechanism (Barrett et al., 1999), the thrust force computed during simulation is shown in Fig. 4 (b) for both shedding schemes. The thrust T and power P are nondimensionalized by the stagnation pressure and the wetted surface area, or $C_T = T/0.5\rho U^2 S$ and $C_P = P/0.5\rho U^3 S$. A summary of these results is given in Table 1. The caudal shedding scheme shows good comparison to the experimental results and high propulsive efficiency $\eta = \overline{T}U/\overline{P}$. The caudal fin and backbone ridge wake shedding scheme also shows high propulsive efficiency, with slightly higher values for the thrust produced and the power required for swimming. This suggests that the interactions of the oscillating tail with upstream-generated vorticity enhances the thrust produced by the tail and the overall performance of the motions.

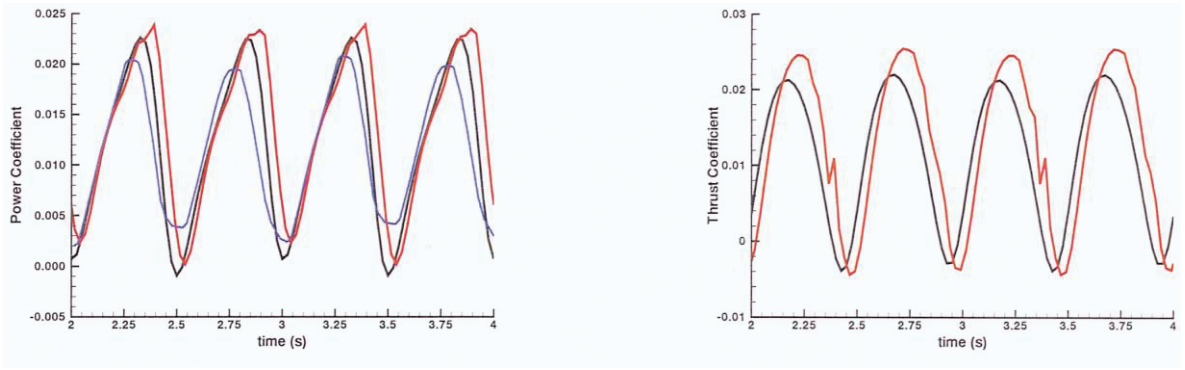

(a) Power coefficient (b) Thrust coefficient

Fig. 4. Time records of (a) the total power coefficient C_P into the fluid and (b) the total thrust coefficient C_T. Comparison of the various methods: (i) caudal fin shedding only (black); (ii) caudal fin and backbone ridge shedding (red); (iii) experimental measurements of total power from *RoboTuna* (blue). Summary of principal performance measures is given in Table 1.

Table 1. Summary of performance data, showing comparison between experimental measurements from *RoboTuna*, wake shedding Scheme A (caudal fin shedding only), and wake shedding Scheme B (caudal fin and backbone ridge shedding).

		RoboTuna	Scheme A	Scheme B
Mean power coefficient	(C_P)	0.0105	0.0113	0.0128
Mean power input difference	(exp. vs. comp.)	—	7.48%	21.5%
Peak power coefficient	(C_P)	0.0194	0.0223	0.0238
Peak power input difference	(exp. vs. comp.)	—	14.6%	22.2%
Mean thrust coefficient	(C_T)	—	0.0103	0.0118
Computational propulsive efficiency	(h)	—	91.4%	91.8%

4. Discussion

A three-dimensional unsteady flexible-body numerical method has been developed in order to study the near-body flow kinematics and performance of fish swimming motions. The simulations of the *RoboTuna* geometry and kinematics show good comparison to the experimentally measured motions. The unsteady propulsion mechanisms utilized by fish are elucidated through the visualization of the near-body and wake structure dynamics. The steadily-swimming fish generates vorticity through the body undulations described by a progressive backbone wave. This body-generated vorticity interacts with the strong wake shed from the oscillating caudal fin to affect the efficient generation of a thrust jet in the form of a reverse Kármán vortex street. Low pressure regions formed by the acceleration of the near-body fluid by the backbone wave are manipulated by the oscillating tail to enhance the strength of the thrust jet, as well as to recover energy from the flow through increased localized lift around the tail. These fluid actuation and transport processes are significantly affected by variation of the prescribed body kinematics; thus, this investigation of unsteady propulsion schemes uniquely lends itself to comprehensive visual study.

Acknowledgments

Financial support of the Office of Naval Research under contract N00014-96-1-1141 monitored by P. Purtell, T. McMullen & J. Fein; the Office of Naval Research under grants N00014-89-J-3186 and N00014-93-1-0774; the Advanced Research Project Agency under contract numbers N00014-92-1726 and N00014-94-1-0735; and the Sea Grant Program under Grant Number NA46RG0434 is gratefully acknowledged.

References

Aleyev, Y., Nekton, Dr. W. Junk b.v., Publishers, The Hague, Netherlands (1977).

Anderson, J., Vorticity control for efficient propulsion, Doctoral Thesis, Massachusetts Institute of Technology and the Woods Hole Oceanographic Institution (1996).

Anderson, J., Streitlien, K., Barrett, D. and Triantafyllou, M., Oscillating foils of high propulsive efficiency, Journal of Fluid Mechanics, 360 (1998), 41-72.

Barrett, D., Propulsive efficiency of a flexible hull underwater vehicle, Doctoral Thesis, Massachusetts Institute of Technology(1996).

Barrett, D., Triantafyllou, M., Yue, D., Grosenbaugh, M. and Wolfgang, M., Drag reduction in fish-like locomotion, Journal of Fluid Mechanics, 392 (1999), 183-212.

Blake, R.W., Fish locomotion (1983) Cambridge University Press,Cambridge.

Chopra, M., Large amplitude lunate-tail theory of fish locomotion, Journal of Fluid Mechanics, 74 (1976), 161-182.

Chopra, M. and Kambe, T., Hydromechanics of lunate-tail swimming propulsion. Part 2., Journal of Fluid Mechanics, 79 (1977), 49-69.

Dewar, H. and Graham, J., Studies of tropical tuna swimming performancein a large water tunnel. III. Kinematics, Journal of Experimental Biology, 192 (1994), 45-59.

Domenici, P. and Blake, R., Review: The kinematics and performance of fish fast-start swimming, Journal of Experimental Biology, 200 (1997),1165-1178.

Ellington, C.P., The aerodynamics of hovering insect flight. IV. Aerodynamic mechanisms, Philosophic Transactions of the Royal Society London, B 305 (1984), 79-113.

Fierstine, H.L. and Walters, V., Studies in locomotion and anatomy of scombroid fishes, Memoir to the Southern California Academy of Sciences, 6 (1968), 1-31.

Gopalkrishnan, R., Triantafyllou, M., Triantafyllou, G. and Barrett, D., Active vorticity control in a shear flow using a flapping foil, Journal of Fluid Mechanics, 274 (1994), 1-21.

Gray, J., Studies in animal locomotion: VI. The propulsive powers of the dolphin, Journal of Experimental Biology, 13:2 (1936), 192-199.

Harper, D. and Blake, R.W., Fast start performance of rainbow trout Salmo gairdneri and northern pike Esox lucius during escapes, J. Exp. Biol., 150 (1989), 321-342.

von Kármán, T. and Burgess, J., General aerodynamic theory - Perfect fluids, in Aerodynamic theory: Volume 2 (1935) W. Durand ed., Springer-Verlag, Berlin, 346-349.

Katz, J. and Plotkin, A., Low-speed aerodynamics: From wing theory to panel methods (1991) McGraw-Hill, Inc., Series in Aeronautical and Aerospace Engineering, New York, NY.

Krasny, R., Desingularization of periodic vortex sheet roll-up, Journal of Computational Physics, 65 (1986), 292-313.

Lan, C., The unsteady quasi-vortex-lattice method with applications to animal propulsion, Journal of Fluid Mechanics, 93 (1979), 747-765.

Lighthill, M., Mathematical Biofluiddynamics, Society for Industrial and Applied Mathematics, Philadelphia, Pennsylvania (1975).

Liu, H., Wassenberg, R. and Kawachi, K., The three-dimensional hydrodynamics of tadpole swimming, Journal of Experimental Biology, 200 (1997), 2807-2819.

Müller, U., van den Heuvel, B., Stamhuis, E. and Videler, J., Fish foot prints: Morphology and energetics of the wake behind a continuously swimming mullet (Chelon labrosus Risso), Journal of Experimental Biology, 200 (1997), 2893-2906.

Streitlien, K., Triantafyllou, G. and Triantafyllou, M., Efficient foil propulsion through vortex control, AIAA Journal, 34:11 (1996),2315-2319.

Taneda, S. and Tomonari, Y., An experiment on the flow around a waving plate, J. Phys. Soc. Japan, 36:6 (1974), 1683-1689.

Triantafyllou, M., Triantafyllou, G. and Gopalkrishnan, R., Wake mechanics for thrust generation in oscillating foils, Phys. Fluids A,3 (1991), 2835-2837.

Triantafyllou, G., Triantafyllou, M. and Grosenbaugh, M., Optimal thrust development in oscillating foils with application to fish propulsion, Journal of Fluids and Structures, 7 (1993), 205-224.

Triantafyllou, M., Barrett, D., Yue, D., Anderson, J., Grosenbaugh, M., Streitlien, K. and Triantafyllou, G., A new paradigm of propulsion and maneuvering for marine vehicles, SNAME Trans., 104 (1996), 81-100.
Videler, J., Fish Swimming, Chapman and Hall, London (1993).
Videler, J. and Hess, F., Fast continuous swimming of two pelagic predators, saithe (Pollachius virens) and mackerel (Scomber scombrus): A kinematic analysis, Journal of Experimental Biology, 109 (1984), 209-228.
Weihs, D., A hydrodynamical analysis of fish turning manoeuvres, Proceedings of the Royal Society of London, B 182 (1972), 59-72.
Weihs, D., The mechanism of rapid starting of slender fish, Biorheology, 10:10 (1973), 343-350.
Wolfgang, M., Hydrodynamics of flexible-body swimming motions, Doctoral Thesis, Massachusetts Institute of Technology (1999).
Wolfgang, M., Anderson, J., Grosenbaugh, M., Yue, D. and Triantafyllou,M., Near-body flow dynamics in swimming fish, Journal of Experimental Biology, 202 (1999), 2303-2327.
Wu, T., Swimming of waving plate, Journal of Fluid Mechanics, 10(1961), 321-344.
Wu, T., Hydromechanics of swimming propulsion. Parts 1-3, Journal of Fluid Mechanics, 46 (1971)

Authors' Profiles

Meldon J. Wolfgang IV : He received his Ph.D. in hydrodynamics from the Department of Ocean Engineering at the Massachusetts Institute of Technology in April, 1999. Prior to that, he received his B.S. in Naval Architecture and Marine Engineering from the Webb Institute of Naval Architecture in 1993. He is currently a research engineer in the M.I.T. Ocean Engineering Department, and his research interests include flexible-body hydrodynamics, active flow control, and computational vortex methods.

Michael S. Triantafyllou : He was born and raised in Athens, Greece. Undergraduate studies at the National Technical University of Athens (1969-74), graduate studies at MIT: SM in Ocean Engineering and SM in Mechanical Engineering (1977), ScD in 1979. With the MIT faculty since 1979; currently Professor of Ocean Engineering, Director of the Testing Tank Facility, Chairman of the Joint Committee in Applied Ocean Sciences and Engineering, MIT/WHOI Joint Program in Oceanography. Research work focuses on: The mechanics of cables. Vortex induced vibration of bluff bodies. Generation and control of vorticity for flow control. Biomimetic development of vehicles employing unsteady propulsion and maneuvering (work on RoboTuna highlight paper 1995, Scientific American).

Dick K.P. Yue : He received all his degrees (S.B., S.M. and Sc.D.) from M.I.T. He has been a faculty member at M.I.T. since 1983 and is now Professor of Hydrodynamics and Ocean Engineering. He is also Director of the M.I.T. Vortical Flow Research Laboratory, and Associate Director of the M.I.T. Testing (Tow) Tank Facility. His main research interests are: nonlinear wave hydromechanics; free-surface vortical and turbulent flows; fish hydromechanics and vortex dynamics of moving flexible bodies; and computational methods for engineering mechanics. He is the author or co-author of over 100 publications in these areas.